# Predicting the Failure of Ultrasonic Spot Welds by Pull-out from Sheet Metal

Bin Zhou,[1] M. D. Thouless,[1,2] and S. M. Ward[3]

[1]*Department of Mechanical Engineering*
[2]*Department of Material Science and Engineering*
*University of Michigan*
*Ann Arbor, MI, 48109*

[3]*Scientific Research Laboratory*
*Ford Motor Company*
*Dearborn, MI, 48124*

**Abstract**

A methodology for determining the cohesive facture parameters associated with pull-out of spot welds is presented. Since failure of a spot weld by pull-out occurs by mixed-mode fracture of the base metal, the cohesive parameters for ductile fracture of an aluminum alloy were determined and then used to predict the failure of two very different spot-welded geometries. The fracture parameters (characteristic strength and toughness) associated with the shear and normal modes of ductile fracture in thin aluminum alloy coupons were determined by comparing experimental observations to numerical simulations in which a cohesive-fracture zone was embedded within a continuum representation of the sheet metal. These parameters were then used to predict the load-displacement curves for ultrasonically spot-welded joints in T-peel and lap-shear configurations. The predictions were in excellent agreement with the experimental data. The results of the present work indicate that cohesive-zone models may be very useful for design purposes, since both the strength and the energy absorbed by plastic deformation during weld pull-out can be predicted quite accurately.

*Keywords:* ultrasonic spot weld, nugget pull-out, sheet metal, cohesive zone, fracture, cohesive strength, toughness.

(March 2006)

## 1. Introduction

Ultrasonic spot-welding has been recognized as a promising technology in joining automotive sheet metal. Compared to conventional resistance spot-welding techniques, ultrasonic welding provides a low-energy bonding technique, and is especially suitable to join aluminum alloys [Hetrick *et al.*, 2005]. Ultrasonic vibrations of a specially designed welding tip can lead to a solid-state bond across the interface between two components without any melting of the alloy [Harthoorn, 1978]. Pioneering work on the technology indicated that the quality of ultrasonic welds is sensitive to several crucial process parameters, such as the welding energy and time [Jones and Meyer, 1958; Harthoorn, 1978; Hazlett and Ambekar, 1970; Matsuoka, 1995; Tsujino *et al.*, 2002]. The primary focus of the present work is to model nugget pull-out using an ultrasonic spot weld as a model system.

Two common failure modes for spot welds are pull-out of the nugget, where the weld is torn away from the base metal along the circumference of the weld nugget, and fracture of the nugget (interfacial fracture between the two adherends). While the transition between the two failure modes depends on the geometry, the size of the welds, and the quality of the weld [Cavalli *et al.* 2005], nugget fracture is generally not acceptable in welding practice. A sound weld is considered to be one that fails by pull-out. Therefore, nugget pull-out is generally seen as being of more practical interest, and is the failure mechanism considered in this paper. A micrograph of this mode of failure can be seen in Fig. 12(c).

Most previous studies on the strength of spot welds have employed *strength-based* approaches, where mixed-mode failure criteria are formulated in terms of the local

loads acting on the welds and the appropriate strengths of the weld [Lee *et al*. 1998; Wung, 2001; Wung *et al.*, 2001, Lin *et al*., 2002; Lin *et al*., 2003; Chao, 2003; Lee *et al*., 2005]. A limitation of these approaches is that fracture generally involves considerations of energy in addition to considerations of strength, and, therefore, purely strength-based approaches to fracture are not expected to give geometry-independent predictions. There have also been studies that have approached the problem of weld failure from an *energy-based* approach, using linear-elastic fracture-mechanics [Zhang, 1997, 1999, 2001; Lee *et al.*, 2005]. However, these approaches are limited to systems dominated by elasticity or small-scale yielding (small compared to the thickness of the sheet metal and to the size of the weld). They cannot be used to provide the complete knowledge of load-deformation relationships required for energy-management considerations when welds fail in plastically deforming joints. Other approaches include design-of-experiments methods to deduce the effects of different parameters on the quality of spot welds [Zhou *et al.*, 2003], and the use of a parametric damage model for the weld [Langrand and Combescure, 2004].

Cohesive-zone models [Needleman, 1987; Tvergaard and Hutchinson, 1992] combine *strength* and *energy* parameters, and have been shown to provide an excellent tool for characterizing the entire fracture process from crack initiation to final catastrophic failure. The models can be used to describe fracture associated with elastic deformation and fracture associated with plastic deformation. Techniques for evaluating the strength and energy parameters for cohesive-zone models have been demonstrated for mixed-mode fracture of adhesively-bonded metals (Yang and Thouless, 2001; Kafkalidis and Thouless, 2002), and mode-I fracture of metal alloys (Li and Siegmund, 2002,

Chabanet, 2003, Roy and Dodds, 2001, Chen *et al.*, 2003). Furthermore, recent work on resistance spot welds [Cavalli and Thouless, 2005], weld-bonded sheet metal [Cavalli and Thouless, 2004], and nugget fracture of ultrasonic spot welds [Zhou *et al.*, 2005] has shown that the cohesive-zone approach has the potential to provide accurate numerical predictions for plastic load-displacement curves obtained during the failure of spot welds. In particular, the work of Cavalli and Thouless [2005] demonstrated that the predictive ability shown by this approach suggests it may be able to form the basis of a robust design methodology that would allow strengths, energy-absorption and failure mechanisms to be predicted for different geometries.

An important issue in the use of cohesive-zone analyses is how to determine the important fracture parameters, strength and toughness, that are needed for each mode of each failure mechanism. While there do appear to be some systems [Li *et al.*, 2005] for which a single experiment suffices to determine both the strength and toughness parameters for one mode of fracture, it appears that, generally, a unique pair of cohesive fracture parameters may not be determined through matching the test data with finite-element predictions for a single geometry [Roy and Dodds, 2001, Zhou *et al.*, 2005]. This has led to different approaches to determine suitable values for the parameters. To analyze crack growth in thin sheet metal, Li and Siegmund [2002] assumed that the cohesive strength of a metal is twice the yield strength. Roy and Dodds [2001] equated the toughness to the small-scale-yielding value. Chen *et al.* [2003] estimated the toughness of a thick compact-tension specimen by topographical measurements of the dimple height on a fracture surface, and subsequently determined the cohesive strength by fitting experimental data. In their analysis of spot welds, Cavalli and Thouless [2005]

assumed that the cohesive strengths of an aluminum alloy and of a resistance spot weld between two sheets of the alloy were given by the tensile strength of the alloy. The toughness could then be determined from numerical fits to experimental data for the load-displacement curves obtained from a welded joint. Zhou *et al.* [2005] determined the mode-I strength and toughness for nugget fracture of an ultrasonic weld by matching numerical fits to experimental load-displacement data for multiple geometries. It is this latter approach that is used in the present investigation of weld pullout, which is intended to address the deficiency of the earlier work by Cavalli and Thouless [2005] in which cohesive strengths were equated to the tensile strength of the base alloy.

The work of Cavalli and Thouless [2005] demonstrated that simulation of mixed-mode fracture during nugget pull-out requires the simultaneous determination of multiple cohesive parameters - the cohesive strength and toughness associated with each of the three modes of fracture. Even with an assumption that the mode-II and mode-III fracture properties are identical, which reduces the number of required parameters to four, a simultaneous measurement of the parameters is quite daunting. Therefore, in the present work, it was assumed that the cohesive parameters of the parent aluminum alloy could be directly measured and used to describe fracture along the weld boundary. This approach contains an implicit assumption that the welding process causes no significant change to the fracture properties of the material surrounding the nugget. This assumption was initially justified because ultrasonic welding is a low-temperature process that does not induce a significant heat-affected zone. Micro-hardness measurements through sections of the weld and the neighboring metal [Zhou *et al.*, 2005] showed no obvious differences in mechanical properties between the weld region and the parent metal. Finally,

validation of the predictive nature of the analysis confirmed this was a reasonable assumption to have made.

In the work that is described in the following sections, multiple fracture tests on thin sheets of aluminum alloy in the absence of any welds were used to determine the four fracture parameters for ductile fracture. These parameters were then used in cohesive-zone analyses to predict the behavior of two different joints bonded by ultrasonic welds failing by pull-out and deforming by extensive plasticity. The quality of the predictions was striking, especially given the fact that the two joint geometries used for model validation were completely unrelated to the test geometries used to determine the properties of the base material.

## 2. Finite-element modeling

All analyses described in this paper were done using the commercial finite-element code ABAQUS®. Mesh-sensitivity analyses were conducted to ensure that the numerical error associated with any quoted results was smaller than the uncertainties associated with the experimental data or material properties. The continuum properties of the base metal (a 0.9 mm thick sheet of AA6111-T4 aluminum alloy) were directly incorporated into the modeling as a point-by-point representation of an experimentally determined tensile stress-strain curve for the alloy. The base metal was assumed to be isotropic and to follow a von Mises yield criterion. It was modeled by a refined mesh of continuum 3-D brick elements. The hardening effect in any region where the sheet metal was bent during the fabrication process was included in the analyses by conducting a separate finite-element calculation to determine the initial plastic-strain field.

All the fracture processes were incorporated into the analyses by means of 3-D, mixed-mode, user-defined, cohesive-zone elements. While details of related codes to describe these elements are provided by Yang [2000] and Cavalli [2003], a summary of the essential points is presented here. The cohesive elements were placed along the expected fracture planes. For example, as shown in Fig. 1(a), the cohesive-zone elements were placed all around the interface between the nugget and the surrounding base material when analyzing nugget pull-out. As shown in that figure, two surfaces of the cohesive elements were formed by nodes belonging to the continuum elements on either side of the fracture plane. Relative displacements between pairs of nodes in the cohesive element could occur in three dimensions, independently of the other nodes, causing 3-D deformation of the element. The normal and shear displacements between each pair of nodes were linked to the normal and shear tractions, $\sigma$ and $\tau$, by means of a trapezoidal traction-separation law shown in Fig. 1b. This trapezoidal shape was chosen as it approximately mimics the elastic-plastic behavior of the alloy. The mode-I law was characterized by a characteristic cohesive strength, $\hat{\sigma}$, and a fracture toughness, $\Gamma_I$. The mode-II and mode-III laws were identical to each other and were characterized by a characteristic strength, $\hat{\tau}$, and a fracture toughness, $\Gamma_{II}$. Following the work of Yang and Thouless [2001], the shear cohesive properties were assumed to be completely independent of the normal cohesive properties, since it was observed during that study that mode-independent properties were required for good predictive capability. The shape parameters for both modes, $\lambda_1 = 0.01$ and $\lambda_2 = 0.5$, were selected to ensure an appropriate level of elastic stiffness upon loading, and to avoid numerical instabilities during unloading. For fracture in a single mode of loading, failure of a node pair was

defined as occurring when the separation reached a critical value, $\delta_c$, or, equivalently, when the crack-driving force $\mathcal{G}$ equaled the toughness, $\Gamma$. At this stage, the node pair no longer supported a load, and the crack was considered to have advanced. For mixed-mode fracture, a simple mixed-mode failure criterion was adopted to couple the various modes of loading [Yang and Thouless, 2001]:

$$\frac{\mathcal{G}_I}{\Gamma_I} + \frac{\mathcal{G}_{II}}{\Gamma_{II}} + \frac{\mathcal{G}_{III}}{\Gamma_{III}} = 1 \quad , \tag{1}$$

where $\mathcal{G}_I$, $\mathcal{G}_{II}$ and $\mathcal{G}_{III}$ are the energy-release rates associated with each mode.

## 3. Fracture parameters of aluminum thin sheet

Four different experiments were developed to determine the fracture properties of the 0.9 mm thick sheet of AA6111-T4 aluminum alloy used as a base metal for the ultrasonic welding. The fracture properties were determined by fitting the results of 3-D, cohesive-zone, finite-element analyses for each test to the appropriate experimental data. The mode-I parameters were determined from tensile tests on deep-notched specimens and compact-tension tests. The mode-II parameters were determined from shear tests on deep-notched specimens and trouser tests. These tests all resulted in fracture being accompanied by extensive plastic deformation, as is appropriate for pull-out of spot welds from the sheet metal. The details of the experiments and the fitting procedures are described below.

### *3.1 Mode-I fracture parameters*

Mode-I fracture of sheet metal has been very extensively studied. Two-dimensional, plane-stress, finite-element models (or hybrid models with both plane-stress and plane-strain elements) can be used to predict the fracture behavior of sheet metal [Li

and Siegmund, 2002, Chabanet, 2003]. However, even the relatively low levels of stress triaxiality at the crack tip in thin specimens [Li and Siegmund, 2002; Pardoen *et al.*, 2004; Roy and Dodds, 2001; Gullerud *et al.*, 1999] may cause crack tunneling, which essentially renders the fracture 3-D in nature. Additionally, medium to high ductility aluminum alloys may exhibit local necking in mode-I tests, which cannot be effectively captured in a 2-D analysis. Therefore, in the present study, 3-D finite-element analyses and 3-D cohesive models were used to model the behavior of the aluminum. While it is recognized that constraint effects may cause the fracture parameters to vary across the section [Chen *et al.*, 2003], average properties are used in this study. Furthermore, any possible effects of thickness on the properties are neglected, as only one thickness of sheet metal was used in this study.

3.1.1 Deep-notched tensile test

Deep-notched tensile test specimens were prepared with dimensions shown in Fig. 2a. A shallow scribe mark was made with a sharp razor along the middle of the ligament to guide the fracture path. The specimens were clamped by wedge grips and loaded on a screw-driven tensile test machine at a rate of 1 mm/min. A CCD camera took a series of images of the tests so that the cross-head displacement could be calibrated. Post-failure examination of the fracture surface (Fig. 2b) indicated that there was only a limited amount of necking (the thickness of the sheet was reduced from 0.9 mm to about 0.8 mm), and the fracture surfaces were relatively flat - confirming mode-I fracture. The resultant load-displacement plots are presented in Fig. 3a. Finite-element analyses with a cohesive zone embedded along the centre of the ligament were performed with a range of cohesive parameters. It was noted that the peak load resulting from these simulations

was independent of toughness, and depended only on the cohesive strength chosen for the cohesive zone. This is probably associated with the small size of the ligament which results in the stress distribution being relatively uniform along the fracture plane. Figure 3a also compares the results of these cohesive-zone calculations to the experimental results, showing that a cohesive strength of $\hat{\sigma}_p = 310 \pm 10$ MPa provides a good fit to the peak load. As can be seen from Fig. 3b, different values of toughness affect only the displacement that is obtained after the peak load. Fitting these displacements may not be a very sensitive way of deducing the toughness but, within the limitations of this approach, it was noted that a value of approximately $\Gamma_I = 50$ kJm$^{-2}$ resulted in predicted displacements that were consistent with the experimental observations. This combination of cohesive properties ($\Gamma_I = 50$ kJm$^{-2}$ and $\hat{\sigma}_p = 310$ MPa) also resulted in the numerical simulations reproducing the extent of necking observed at fracture.

3.1.2 Compact-tension test

Compact-tension tests are generally useful for determining the toughness of a material, because relatively large amounts of stable crack propagation can be sustained. Compact-tension specimens were designed as shown in Fig. 4a. The specimens were pin-loaded at a rate of 1 mm/min, with the displacements being calibrated optically. During initial tests, it was noticed that the thin alloy sheets tended to warp because of the compression near the crack tip. This often resulted in a mixed-mode and "slant" fracture along the crack path. Similar observations of out-of-plane bending in compact-tension tests on thin sheet metal and the associated slant fracture have been widely reported [Pardoen *et al.*, 2004; Gullerud *et al.*, 1999; Roy and Dodds, 2001]. Therefore, pads were

applied between the specimen and the pin-loading grips to reduce such out-of-plane deformation. A guide line was scribed along both surfaces of the specimen, to help avoid the slant fracture. As a result, relatively straight and mode-I fracture surfaces were produced, as shown in Fig. 4b. The extent of necking at the fracture surface was similar to that observed for the tensile tests. Load-displacement data from the compact-tension tests are shown in Fig. 5. The results from cohesive-zone analyses for this geometry were fitted to these experimental data. The cohesive strength used in these analyses was maintained at $310 \pm 10$ MPa, as obtained from the tensile tests; the values of the toughness were varied to determine the best fit to the data. These analyses resulted in a value of toughness given by $\Gamma_I = 50 \pm 10$ kJm$^{-2}$, which is essentially identical to the toughness estimated in the previous section. The resulting load-displacement curves are superimposed on the experimental data of Fig. 5. One incidental observation about these computational results is that they predicted some minor crack tunneling, analogous to what was observed experimentally. However, since this was not the primary focus of the present work, these observations were not pursued further.

*3.2 Mode-II and mode-III fracture parameters*

3.2.1 Shear test

A pure mode-II shear test was designed following ASTM standard B831-93, with the purpose of directly measuring the shear strength of the aluminum alloy. The dimensions of the test specimens are shown in Fig. 6a. The specimens were loaded in remote tension by two wedge grips at a displacement rate of 1 mm/min, with the displacements being calibrated optically. In successful tests used for subsequent analyses, the ligament sheared along the central line joining the ends of the notches, and the

fracture surface was flat and relatively smooth (Fig. 6b). The resultant load-displacement plots are shown in Fig. 7a. Superimposed on this figure is a curve that matches the experimental results, and arises from one particular set of cohesive parameters. However, further numerical analysis showed that a range of combinations of mode-II toughness and strength could provide essentially identical curves. In a similar result to that encountered during previous work on nugget fracture [Zhou *et al.*, 2005], there was no unique pair of parameters that could be used to describe fracture during the shear test. For any value of shear strength between about 180 and 230 MPa, a corresponding value of mode-II toughness could be found that would allow a suitable numerical fit to the load-displacement data. The range of shear strengths and toughness that permit a fit to the data (including the experimental variability) is shown in the plot of Fig. 7b.

3.2.2 Trouser test

To produce a tighter set of bounds on the shear toughness and strength, an additional test was devised. This was the "trouser test" with the geometry shown in Fig. 8a. The specimens were prepared using the same coupons of aluminum sheet, with the two legs of the specimen being bent through 90°. A shallow guiding line was scribed along the central axis between the two legs, to reduce the possibility of mixed-mode slant fracture. The two legs were then clamped in wedge grips, and loaded in a tensile testing machine at a rate of 5 mm/min. This resulted in pure mode-III tearing of the specimen along the central line (Fig. 8b). The resultant load-displacement plot is shown in Fig. 9a. Cohesive-zone analyses were conducted for this test with fracture parameters being selected to provide a good fit to the experimental data. The 3-D nature of these calculations is vividly demonstrated by the image of the deformed mesh shown in Fig. 9b.

A detailed study of this geometry showed that the numerical results were very sensitive to the mode-III toughness, but there was some sensitivity to the shear strength. Including the effects of experimental variability and uncertainty, the range of cohesive parameters that could be fitted to the data is shown in Fig. 10. Superimposed on this plot is the range of shear parameters that provided possible fits to the shear tests of the previous section. Upon assuming that the mode-II cohesive parameters are identical to the mode-III parameters, this superposition results in a small overlapping zone (shaded in Fig. 10) corresponding to a limited range of shear parameters that allows numerical fits to be made to both geometries. This range is taken to be representative of the cohesive parameters that can be used to describe shear fracture of the aluminum sheet. Although the full range of shear parameters spans between 187 and 210 MPa for the strength, $\hat{\tau}$, and between 29 and 44 $kJm^{-2}$ for the toughness, $\Gamma_{II}$, the two parameters are actually coupled within this range. These parameters, combined with the mode-I parameters deduced in the earlier sections, were then used in conjunction with the failure criterion of Eqn. (1) to analyze the mixed-mode fracture associated with nugget pullout.

**4. Prediction of nugget pull-out**

Once the four cohesive parameters of the aluminum alloy had been determined, they were used to predict failure by nugget pull-out in ultrasonic welded joints with two different geometries. At this point, it should be emphasized that no further fits to experimental data were made. The cohesive parameters and material properties were incorporated directly into numerical models of the welded geometries, and the *predictions* that arose from these simulations were compared to the experimental results. Furthermore, it should also be noted that the two geometries used to determine the

cohesive parameters were completely unrelated to the geometries used to test the predictions. The former were simple coupons of sheet metal, the latter were welded joints. Finally, the two welded geometries themselves were very different - as will be evident from an order of magnitude difference in their strengths for essentially identical welds.

The welds studied in this paper were all nominally identical. They were formed under the same conditions, and were rectangular in shape with an approximate size of 5.5 x 7.5 $mm^2$. In the finite-element modeling of both test geometries, the weld nugget consisted of a refined mesh of 3-D hexagonal continuum elements embedded in the thin sheet. The nugget was assigned the same constitutive properties as the rest of the alloy. Three-dimensional cohesive elements (of zero thickness) were placed along all the boundaries between the nugget and the base metal. The traction-separation laws, and the associated shear and normal cohesive parameters, for these elements were identical to those used to describe ductile fracture of the sheet metal. No modifications at all were made to the cohesive elements developed in the previous sections. As always, mesh-sensitivity analyses were conducted to ensure that the size of both the continuum elements and the cohesive-zone elements were fine enough for convergent solutions within the desired level of uncertainty.

*4.1 T-peel test*

T-peel test specimens were prepared using a single ultrasonic weld to bond two 0.9 mm thick AA6111-T4 aluminum coupons together. The coupons were 25 mm wide, 125 mm long, and the center of the weld was 30 mm from one end. In preparing the welds, a rectangular welding tip was used, and the input energy was large enough to

ensure the welds would fail by nugget pull-out. The resultant sizes of the weld nuggets were essentially equal to that of the welding tip (5.5 x 7.5 $mm^2$). After welding, the bonded coupons were bent into the T-peel shape shown in Fig. 11, with a gauge length of 50 mm. A prescribed loading displacement at a rate of 5 mm/min was applied to the specimen by clamping it with wedge grips in a tensile testing machine.

The results of the cohesive-zone analysis for this T-peel geometry are shown in Figs. 12 and 13. Figure 12a shows the numerical predictions for the deformed shape of the geometry during nugget pull-out. Figure 13 presents the numerical predictions of the load-displacement curve, with bounds corresponding to the range of the cohesive parameters. These numerical predictions were then directly compared to experimental observations. The deformed shape and nugget fracture are shown in Fig. 12b. The experimental load-displacement curves are superimposed on Fig. 13. It should be noted that the numerical simulations showed that failure was accompanied by extensive plastic deformation, and was proceeded by initial fracture along the front edge of the weld, followed by tearing along the two sides. This was also observed experimentally. The numerical load-displacement curves displayed two distinct stages of failure: a load drop corresponding to the initial failure of the front edge of the weld, followed by an increase in load as tearing along the sides occurs. From a comparison with the experimental curves, it is clear that the numerical calculations did an excellent job of describing the behavior of the welded joint, with both the qualitative and quantitative features of the load-displacement plot (and hence, the energy absorption of the joint) being predicted.

*4.2 Lap-shear test*

The second welded geometry that was tested was a single-lap-shear joint. These specimens were prepared by joining two coupons of AA6111-T4 sheet metal (25 mm wide and 0.9 mm thick) with an ultrasonic spot weld 30 mm from one end. The gauge length used in the tests was 70 mm, as shown in Fig. 14a. The welding was done with the same welding tip and the same range of input energy as for the T-peel joints. Again, the size of the nugget was approximately 5.5 x 7.5 $mm^2$. Specimens were loaded on a tensile testing machine at a displacement rate of 1 mm/min by griping the two ends in wedge grips. The stiffness of a lap-shear geometry results in displacements that are generally too small to be measured accurately with ease. Rotation and bending that are intrinsic aspects of this test [Kafkalidis and Thouless, 2002] add to the complications of measuring and defining axial displacements. Therefore, it was decided to use the transverse deflection of each arm, as defined in Fig. 14b, as a measurement of displacement. This displacement was measured optically during the experiments.

The predictions of the cohesive-zone analysis for the lap-shear test are shown in Fig. 15. The configuration of the lap-shear test results in large compressive stresses being developed at the rear portion of the spot weld. The numerical modifications necessary to accommodate the extensive local plastic deformation that resulted from this compression were not done, so the numerical calculations were terminated before the final stages of nugget failure. Superimposed on the predictions shown in Fig. 15 are the experimental data for the load and displacement. As can be seen from this figure, the numerical predictions did a good job of predicting the performance of the weld up to the final compressive failure. Until the final portion of the load-displacement curve, where

the load was borne entirely by the compression in the rear portion of the weld, the numerical and experimental curves are in excellent agreement. Figure 16a illustrates the numerical predictions of nugget pull-out that occurs after initial tearing of the front edge of the weld. Complete nugget pullout is shown in the micrograph of Fig. 16b.

It should be noted that the peak load of the lap-shear test was predicted to be an order of magnitude higher than that of the T-peel test, for nominally identical welds and coupons. These predictions accurately captured the experimentally-observed variation in strength. This indicates the power of such an approach, and emphasizes the importance of including both energy and strength terms in the analysis of spot welds. Only with the correct combination of strength and energy parameters, can fracture of spot welds in different joint configurations be successfully predicted.

**5. Concluding remarks**

Four types of fracture experiments were developed to measure the mode-I and mode-II cohesive parameters for ductile fracture of thin sheet metals. A comparison between cohesive-zone analyses and experimental measurements for each test allowed the strength and toughness for the different modes of fracture to be determined. From two mode-I fracture experiments, a deep-notched tensile test and a compact-tension test, the normal cohesive strength and normal toughness of a thin sheet of AA6111-T4 aluminum alloy were determined to be $\hat{\sigma}$=310 ± 10 MPa and $\Gamma_I$= 50 ± 10 kJm$^{-2}$. From shear tests and trouser tests, the shear strength and shear toughness were determined to be in the range of 187~210 MPa and 29~44 kJm$^{-2}$, respectively. These four characteristic fracture parameters were then used in a cohesive-zone analysis of spot weld failure in two distinctly different joints. These analyses successfully predicted pull-out of the weld

when accompanied by extensive plastic deformation. The analyses provided qualitative predictions about the shape of the load-deflection curves, and quantitative predictions about the strength of the joints and the energy dissipated during fracture. The level of agreement between the numerical predictions and the actual performance of the welds was particularly gratifying, since the cohesive parameters had been determined from geometries that were very different from the welded joints. In conclusion, it appears that cohesive-zone analyses with properly calibrated fracture parameters may provide a useful design tool to predict the behavior of spot welds bonding different configurations of sheet metal. If there is no heat-affected zone associated with the welds, then it may be possible that the fracture parameters of the base metal can be used directly to describe the pull-out process.

**Acknowledgements**

Support through the NIST ATP Cooperative Agreement 70NANB3H3015 on ultrasonic metal spot welding is gratefully acknowledged. The authors also thank D. J. Hill, R. Jahn, L. Reatherford, D. Wilkosz, E. Hetrick, A. Grima, and R. Cooper at Ford SRL for their help in this work.

**References**

Standard B831-93 "Standard Test Method for Shear Testing of Thin Aluminum Alloy Products", ASTM, 1998.

Chabanet, O., Steglich, D., Besson, J., Heitmann, V., Hellmann, D. and Brocks, W., "Predicting Crack Growth Resistance of Aluminum Sheets," *Computational Materials Science*, 26, 1-12, 2003.

Cavalli, M. N. and Thouless, M. D., "Cohesive-Zone Modeling of the Deformation and Fracture of Spot-Welded Joints," *Fatigue and Fracture of Engineering Materials and Structures*, **28,** 861-874, 2005.

Cavalli, M. N., "Cohesive-Zone Modeling of Structural Joint Failure," Ph.D. Dissertation, University of Michigan, Ann Arbor, MI, 2003.

Chao, Y., "Ultimate Strength and Failure Mechanism of Resistant Spot Weld Subjected to Tensile, Shear, or Combined Tensile/Shear Loads," *Journal of Engineering Materials and Technology*, **125**, 125-132, 2003.

Chen, C. R., Kolednik, O., Schneider, I., Siegmund, T., Tatschl, A. and Fischer, F. D., "On the Determination of the Cohesive Zone Parameters for the Modeling of Micro-ductile Crack Growth in Thick Specimens," *International Journal of Fracture*, **120**, 517-536, 2003.

Gullerud, A. S., Dodds Jr., R. H., Hampton, R. W. and Dawicke, D. S., "Three Dimensional Modeling of Ductile Crack Growth in Thin Sheet Metals: Computational Aspects and Validation," *Journal of Engineering Fracture Mechanics*, **63**, 347-374, 1999.

Harthoorn, J. L., "Ultrasonic Metal Welding," Ph.D. Dissertation, Technical College Eindhoven, Netherlands, 1978.

Hazlett, T. H. and Ambekar, S. M., "Additional Studies on Interface Temperature and Bonding Mechanisms of Ultrasonic Welds," *Welding Journal*, **49**, 196-200, 1970.

Hetrick, E., Jahn, R., Reatherford, L., Skogsmo, J., Ward, S. M., Wilkosz, D., Devine, J., Graff, K. and Gehrin, R., "Ultrasonic Spot Welding: A New Tool for Aluminum Joining," *Welding Journal*, **84**, 6-30, 2005.

Jones, J. B. and Meyer, F. R., "Ultrasonic Welding of Structural Aluminum Alloys," *Welding Journal*, **3**, 81-92, 1958.

Kafkalidis, M. S. and Thouless, M. D., "The Effects of Geometry and Material Properties on the Fracture of Single Lap-Shear Joints," *International Journal of Solids and Structures*, **39**, 4367-4383, 2002.

Langrand, B. and Combescure, A., "Non-linear and Failure Behavior of Spotwelds: A 'Global' Finite Element and Experiment in Pure and Mixed Modes I/II," *International Journal of Solids and Structures*, **41**, 6631-6646, 2004.

Lee, Y. L., Wehner, T. J., Lu, M. W., Morrissett, T. W. and Pakalnins, E., "Ultimate Strength of Resistance Spot-welds Subjected to Combined Tension and Shear," *Journal of Testing and Evaluation*, **26**, 213-219, 1998.

Lee, H., Kim, N., Lee, T. S., "Over Load Failure Curve and Fatigue Behavior of Spot-Welded Specimens," *Journal of Engineering Fracture Mechanics*, **72**, 1203-1221, 2005.

Li, S, Thouless, M. D., Waas, A. M., Schroeder, J. A. and Zavattieri, P. D., "Use of Mode-I Cohesive-Zone Models to Describe the Fracture of an Adhesively-Bonded

Polymer-Matrix Composite," *Journal of Composites Science & Technology*, **65**, 281-293, 2005.

Li, W. and Siegmund, T., "An Analysis of Crack Growth in Thin Sheet Metal via A Cohesive Zone Model," *Journal of Engineering Fracture Mechanics*, **69**, 2073-2093, 2002.

Lin, S. H., Pan, J., Wu, S. R., Tyan, T. and Wung, P., "Failure Loads of Spot Welds under Combined Opening and Shear Static Loading Conditions," *International Journal of Solids and Structures*, **39**, 19-39, 2002.

Lin, S. H., Pan, J, Tyan, T. and Prasad, P., "A General Failure Criterion for Spot Welds under Combined Loading Conditions," *International Journal of Solids and Structures*, **40**, 5539-5564, 2003.

Matsuoka, S., "Ultrasonic Welding and Characteristics of Glass-Fiber Reinforced Plastic: Comparison between the Paper-making Method and the Impregnation Method," *Journal of Materials Processing Technology*, **55**, 427-431, 1995.

Needleman, A., "A Continuum Model for Void Nucleation by Inclusion Debonding," *Journal of Applied Mechanics*, **54**, 525-531, 1987.

Pardoen, T., Hachez, F., Marchioni, B., Blyth, P. H. and Atkins, A. G., "Mode I Fracture of Sheet Metal," *Journal of the Mechanics and Physics of Solids,* **52**, 423-452, 2004.

Roy, Y.A. and Dodds Jr., R. H., "Simulation of Ductile Crack Growth in Thin Aluminum Panels Using 3-D Surface Cohesive Elements," *International Journal of Fracture*, **110**, 21-45, 2001.

Tsujino, J., Hidai, K., Hasegawa, A., Kanai, R., Matsuura, H., Matsushima, K. and Ueoka, T., "Ultrasonic Butt Welding of Aluminum Alloy and Stainless Steel Plate Specimens," *Ultrasonics*, **40**, 371-374, 2002.

Tvergaard, V. and Hutchinson, J. W. "The Relation Between Crack Growth Resistance and Fracture Process Parameters in Elastic-Plastic Solids," *Journal of the Mechanics and Physics of Solids*, **40**, 1377-1397, 1992.

Wung, P., "A Force-Based Failure Criterion for Spot-weld Design," *Experimental Mechanics*, **41**, 107-113, 2001.

Wung, P., Walsh, T., Ourchane, A., Stewart, W. and Jie, M., "Failure of Spot Welds Under In-Plane Static Loading," *Experimental Mechanics*, **41**, 100-106, 2001.

Yang, Q. D., Thouless, M. D. and Ward, S. M., "Numerical Simulation of Adhesively Bonded Beams Failing with Extensive Plastic Deformation," *Journal of the Mechanics and Physics of Solids*, **47**, 1337-1353, 1999.

Yang, Q. D., Thouless, M. D. and Ward, S. M., "Analysis of the Symmetrical 90°–Peel Test with Extensive Plastic Deformation," *Journal of Adhesion*, **72**, 115-132, 2000.

Yang, Q. D., Thouless, M. D. and Ward, S. M., "Elastic-Plastic Mode-II Fracture of Adhesive Joints," *International Journal of Solids and Structures*, **38**, 3251-3262, 2001.

Yang, Q. D. and Thouless, M. D., "Mixed-Mode Fracture Analysis of Plastically Deforming Adhesive Joints," *International Journal of Fracture*, **110**, 175-187, 2001.

Yang, Q. D., "Fracture Analyses of Plastically-Deforming Adhesive Joints," Ph.D. Dissertation, University of Michigan, Ann Arbor, MI, 2000.

Zhang, S., "Stress Intensity at Spot Welds," *International Journal of Fracture*, **88**, 167-185, 1997.

Zhang, S., "Stress Intensity Derived from Stresses around A Spot Welds," *International Journal of Fracture*, **99**, 239-257, 1999.

Zhang, S., "Approximate Stress Formulas for A Multiaxial Spot Weld Specimen," *Welding Journal*, **80**, 201S-203S, 2001.

Zhou, B., Thouless, M. D. and Ward, S. M., "Mode-I Fracture Parameters in Ultrasonic Spot Welds in Aluminum," (in press) *International Journal of Fracture,* 2005.

Zhou, M., Zhang, H. and Hu, S. J., "Relationships between Quality and Attributes of Spot Welds," *Welding Journal*, **82**, 72S-77S, 2003.

**Figure Captions**

**Figure 1** **(a)** A schematic illustration of how the 3-D cohesive-zone elements are incorporated into a model of weld pull-out. **(b)** A schematic diagram of a trapezoidal traction-separation law used for mode-I. The laws used for mode-II and mode-III fracture had a similar shape.

**Figure 2** **(a)** Geometry and dimensions (in mm) of the deep-notched tensile specimen. The specimens were gripped by wedge grips leaving a gauge length of 10 mm from both sides of the notch. **(b)** Micrographs of a ligament after fracture.

**Figure 3** **(a)** Experimental load-displacement curves with examples of numerical fits using a toughness of 50 $kJm^{-2}$ and a cohesive strength of $310 \pm 10$ MPa. The error in the initial elastic response represents the uncertainty in the optical measurements of displacement used. **(b)** A series of numerical load-displacement curves with a cohesive strength of 310 MPa, showing the effect of different values of toughness.

**Figure 4** **(a)** Geometry and dimensions (in mm) of the compact-tension specimen. **(b)** Micrographs of the failed specimen (from the side, and looking along the crack).

**Figure 5** Comparison between the experimental data and numerical fits to the load-displacement curves from compact-tension tests. These results confirm

values for the mode-I cohesive strength of 310 ± 10 MPa, and the mode-I toughness of 50 ± 10 $kJm^{-2}$.

**Figure 6** **(a)** Geometry and dimensions (in mm) of the shear test specimens. **(b)** Micrographs of the fractured ligament.

**Figure 7** **(a)** Experimental load-displacement curves from the shear test, and an example of a numerical fit to these curves (using a shear strength of 205 MPa and a shear toughness of 35$kJm^{-2}$). **(b)** Range of values of the shear toughness and shear strength that can be used to provide numerical fits to the data of the shear test.

**Figure 8** **(a)** Geometry and dimensions (in mm) of the trouser specimen. **(b)** A micrograph of the deformation of the specimen.

**Figure 9** **(a)** Experimental load-displacement curves for the trouser test, with an example of a numerical fit to the data (using a shear strength of 200 MPa and a shear toughness of 36 $kJm^{-2}$). **(b)** The deformed mesh resulting from the cohesive-zone analysis, illustrating the 3-D nature of the calculations.

**Figure 10** The range of shear fracture parameters that fit the load-displacement curves for the trouser tests. Superimposed on this plot is the range of parameters that allow fits to the shear test. The shaded region illustrates the intersection between these two sets of parameters.

**Figure 11** Geometry and dimensions (in mm) of the welded T-peel specimens.

**Figure 12** **(a)** Deformation and nugget pull-out in T-peel joints predicted by the numerical calculations. **(b)** Micrograph of the deformation in a T-peel joint. **(c)** Micrograph of nugget pull-out in a T-peel joint.

**Figure 13** Predicted load-displacement curve for the welded T-peel joint, compared to experimental results.

**Figure 14** **(a)** Geometry and dimensions (in mm) of the lap-shear geometry. **(b)** Micrograph of a test in progress showing the definition of the transverse deflection of the arms, $U$, used as the measure of displacement in these tests.

**Figure 15** Predicted load-displacement curve for the lap-shear joint, compared to experimental results. Displacements for both curves are the transverse deflections of the arms, as defined in Fig. 14.

**Figure 16** **(a)** Nugget pull-out in the lap-shear joints as predicted by the numerical calculations. **(b)** Nugget pullout as observed experimentally. This micrograph shows the final shear failure at the compressive back surface of the weld nugget.

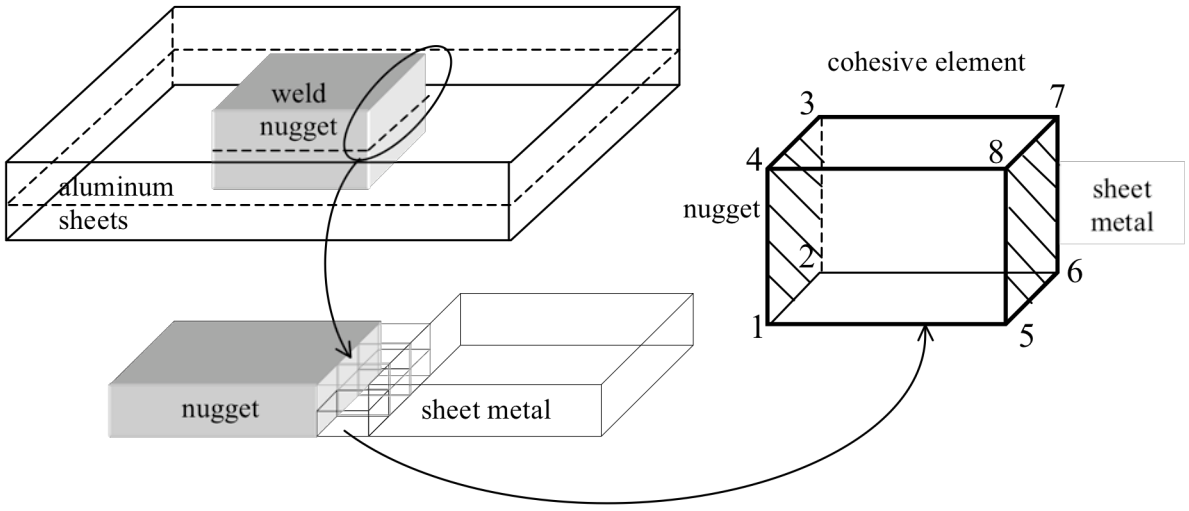
weld
nugget
aluminum
sheets
nugget
sheet metal
cohesive element
3
7
4
8
nugget
sheet
metal
2
6
1
5

**(a)**

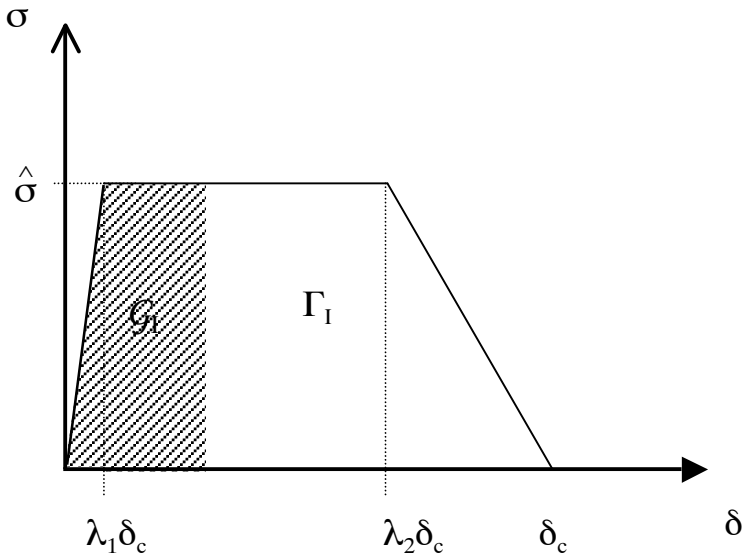
σ
σ̂
$\mathcal{G}_I$
$\Gamma_I$
$\lambda_1\delta_c$
$\lambda_2\delta_c$
$\delta_c$
δ

**(b)**

Figure 1

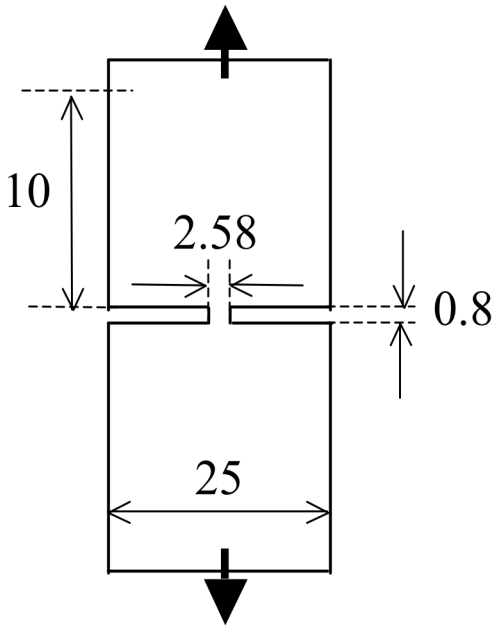


**(a)**

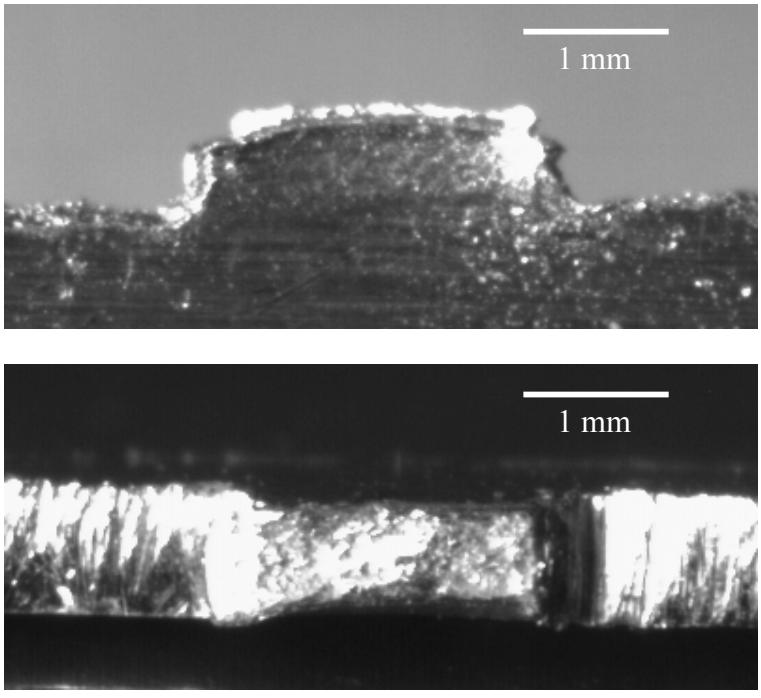


**(b)**

Figure 2

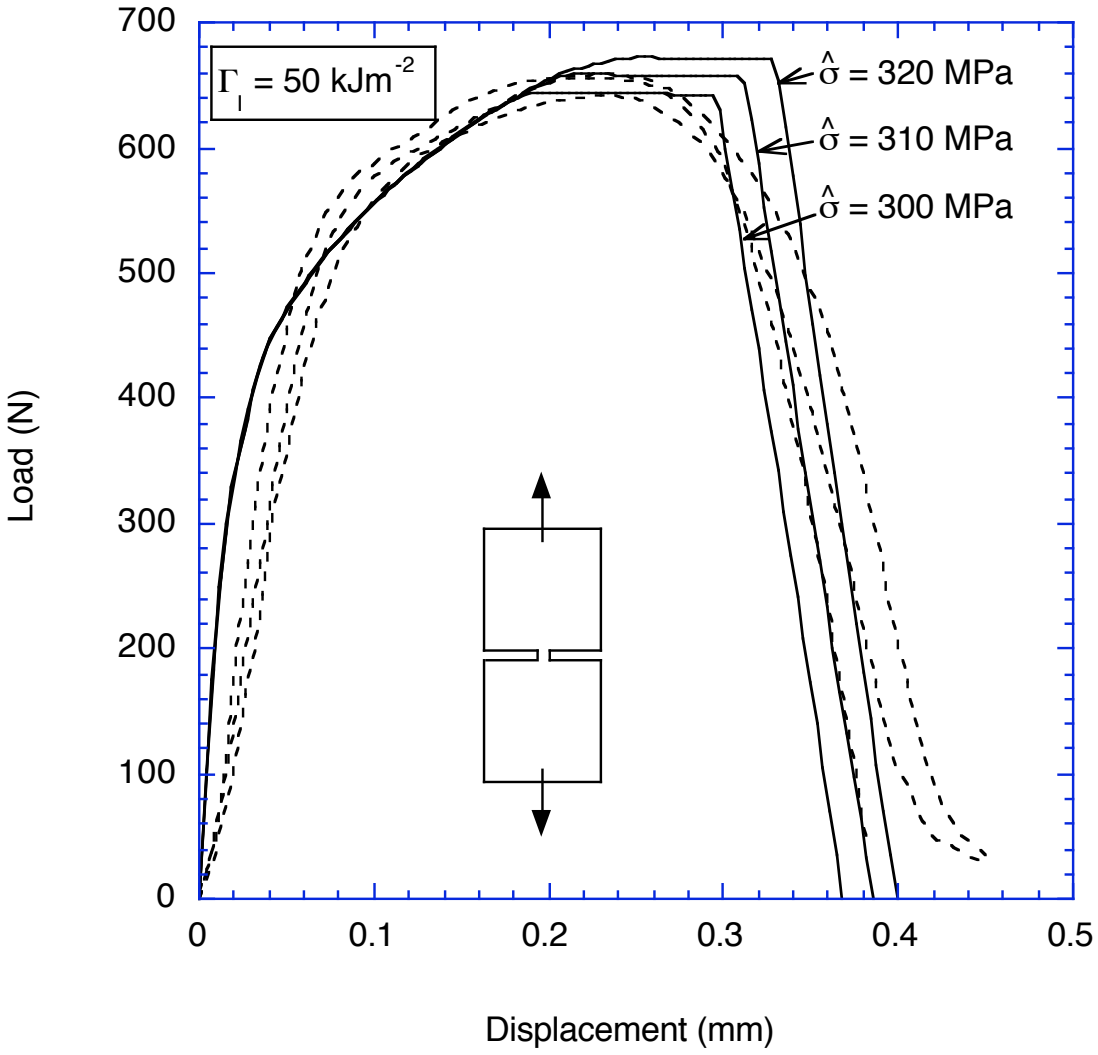
700
600
500
400
300
200
100
0
Load (N)
0
0.1
0.2
0.3
0.4
0.5
Displacement (mm)
$\Gamma_i$ = 50 kJm$^{-2}$
$\hat{\sigma}$ = 320 MPa
$\hat{\sigma}$ = 310 MPa
$\hat{\sigma}$ = 300 MPa

Figure 3a

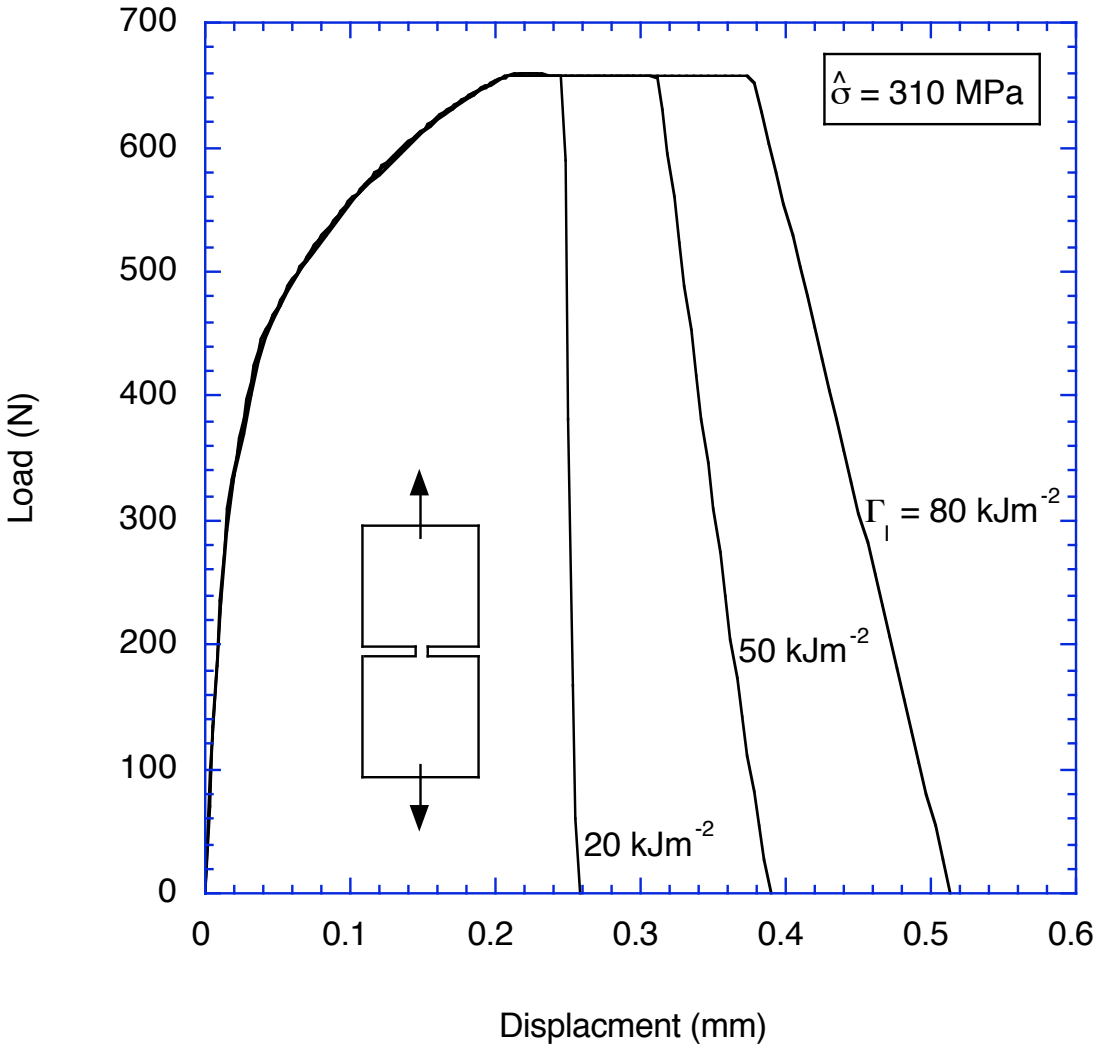
700
600
500
400
300
200
100
0
Load (N)
0
0.1
0.2
0.3
0.4
0.5
0.6
Displacment (mm)
$\hat{\sigma}$ = 310 MPa
$\Gamma_I$ = 80 kJm$^{-2}$
50 kJm$^{-2}$
20 kJm$^{-2}$

Figure 3b

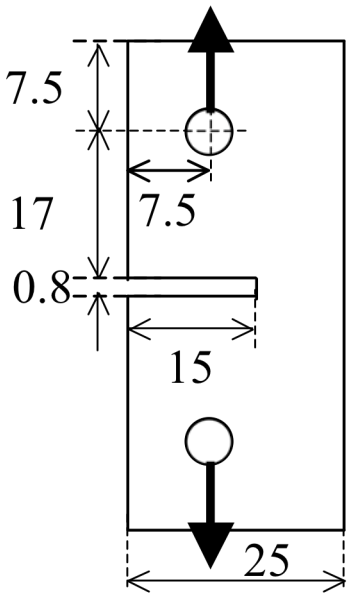


**(a)**

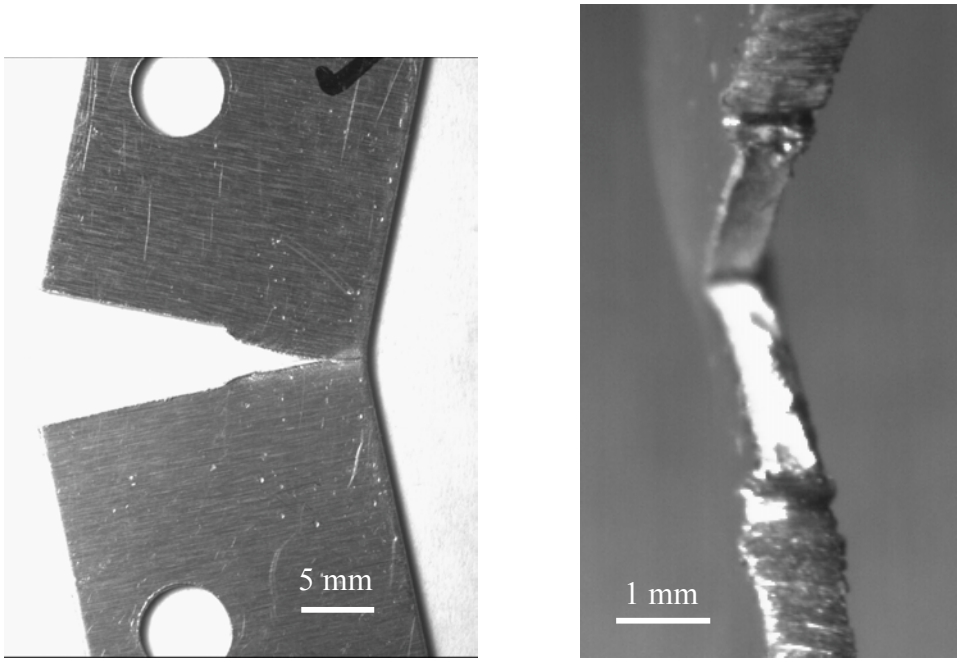


**(b)**

Figure 4

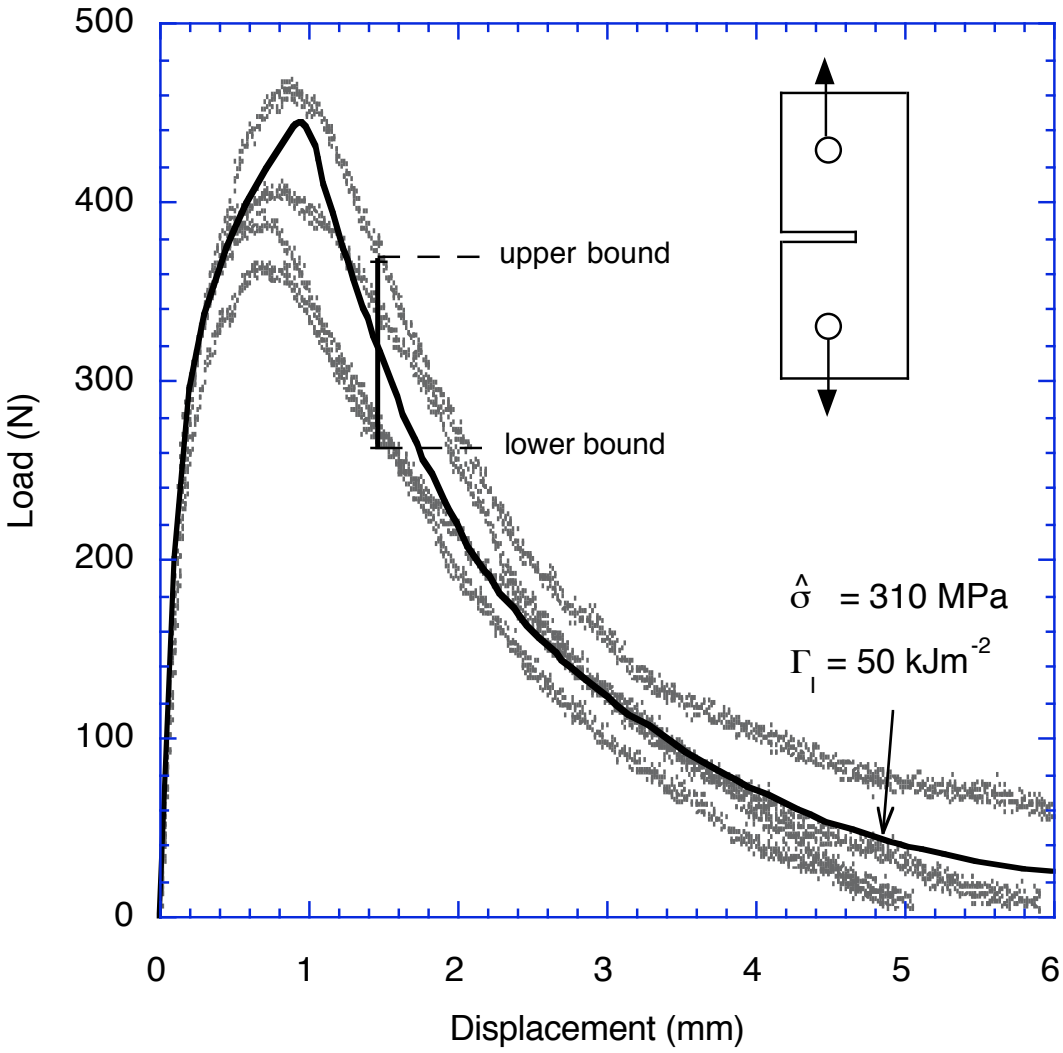
500
400
300
200
100
0
Load (N)
0
1
2
3
4
5
6
Displacement (mm)
upper bound
lower bound
$\hat{\sigma}$ = 310 MPa
$\Gamma_I$ = 50 kJm$^{-2}$

Figure 5

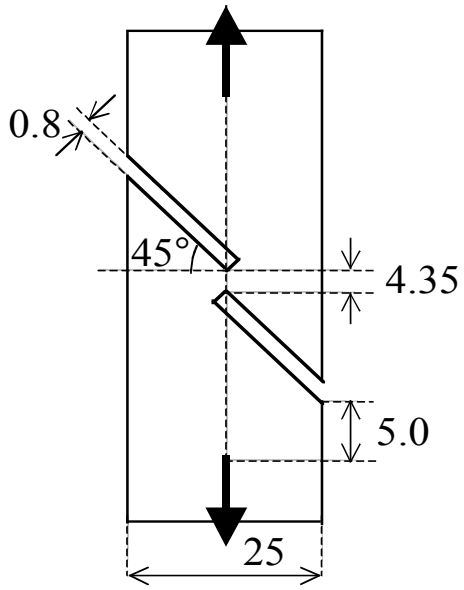


**(a)**

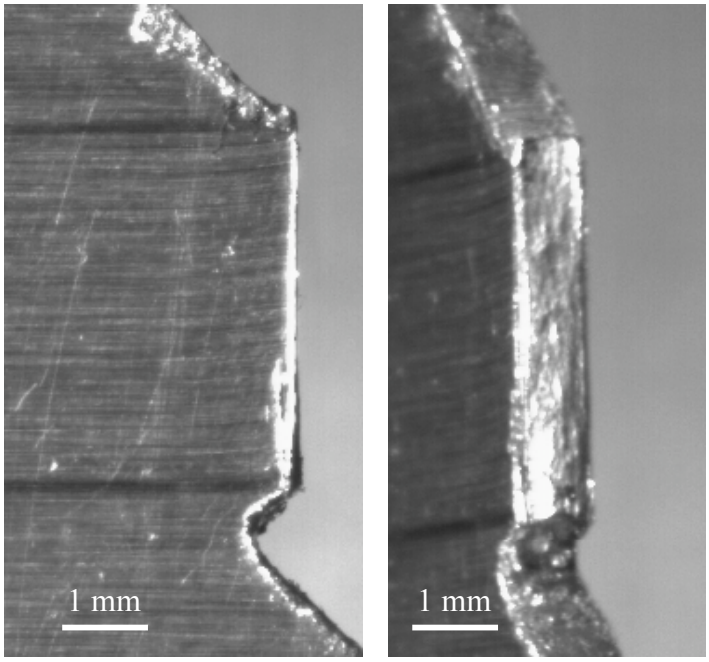


**(b)**

Figure 6

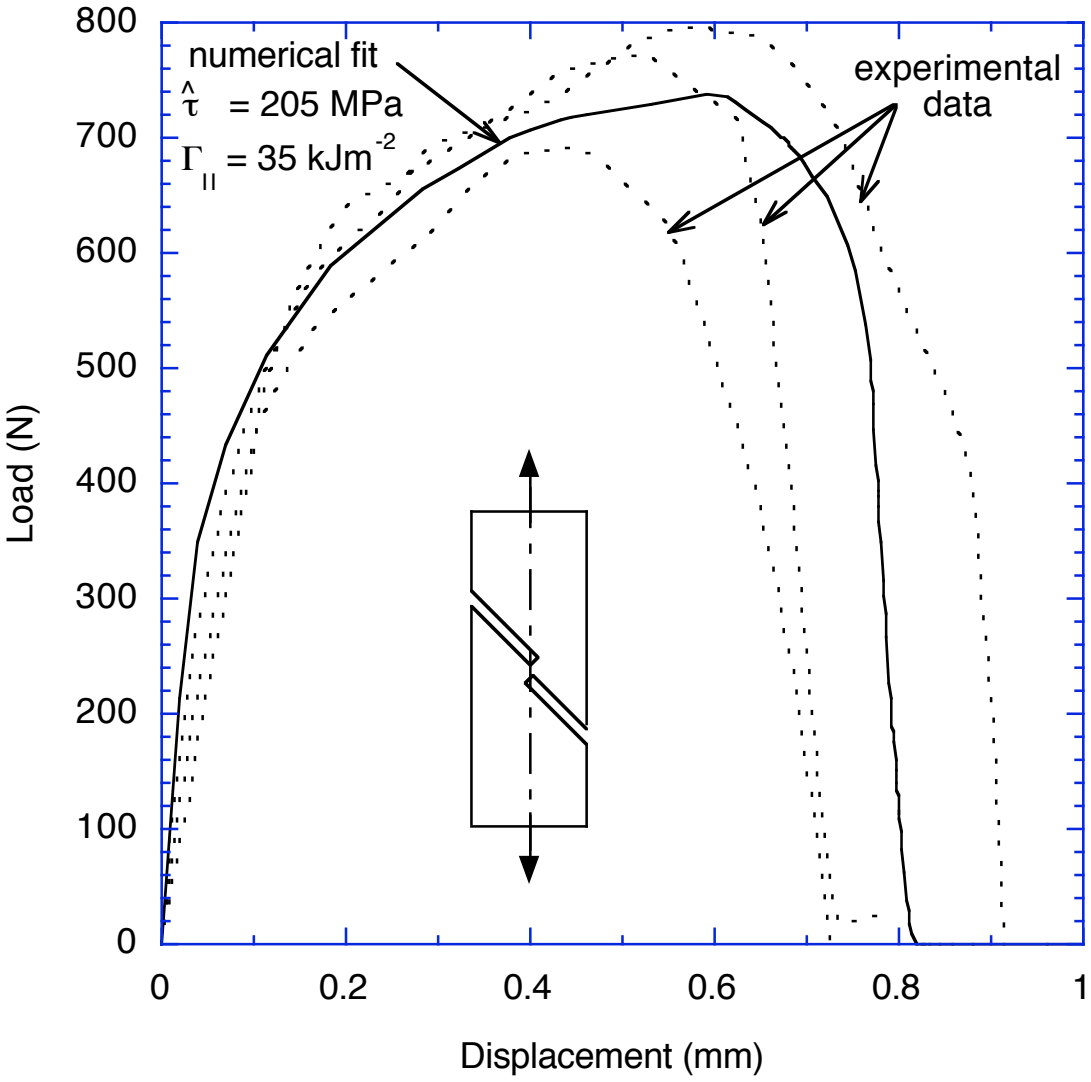
numerical fit
$\hat{\tau}$ = 205 MPa
$\Gamma_{II}$ = 35 kJm$^{-2}$
experimental data
Load (N)
Displacement (mm)
800
700
600
500
400
300
200
100
0
0
0.2
0.4
0.6
0.8
1

Figure 7a

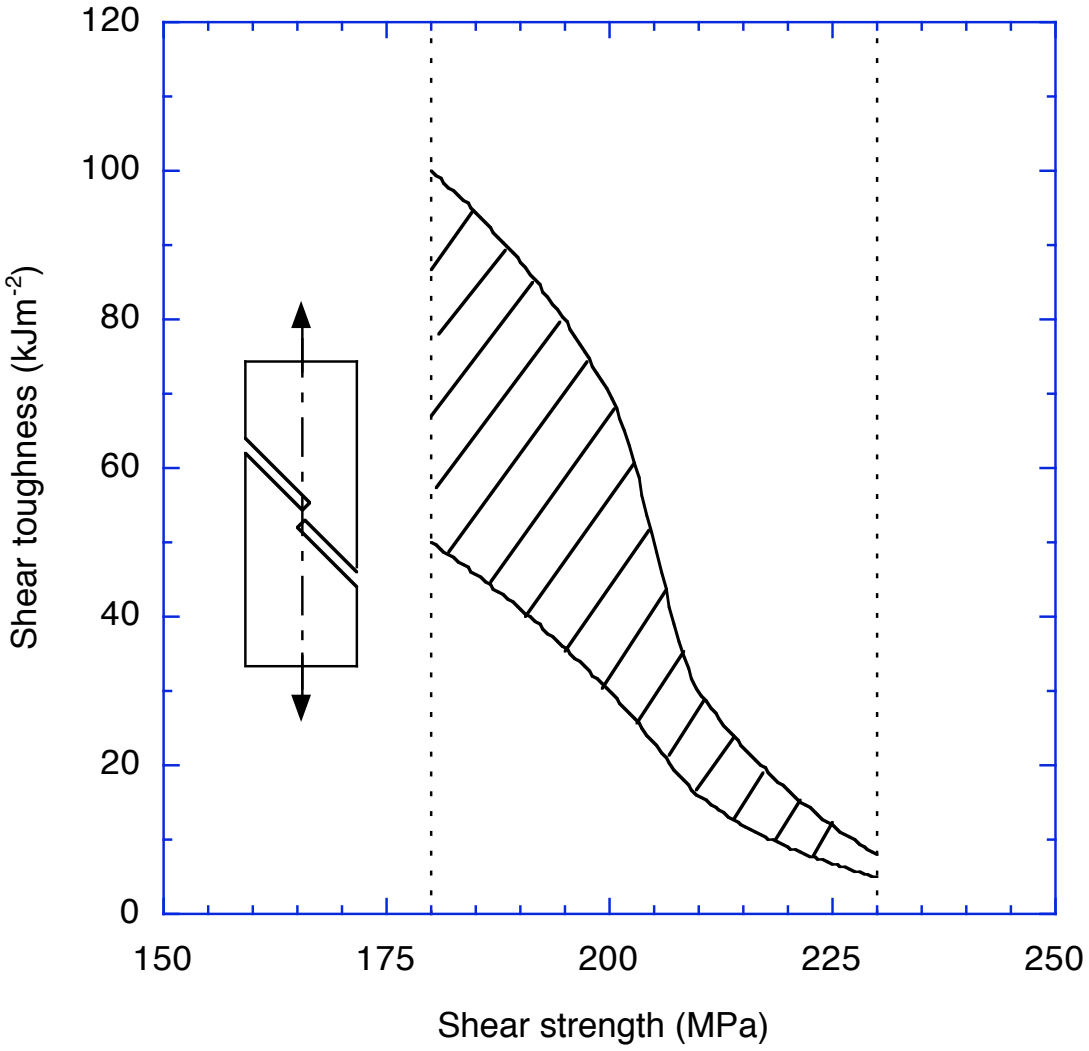
120
100
80
60
40
20
0
Shear toughness (kJm-2)
150
175
200
225
250
Shear strength (MPa)

Figure 7b

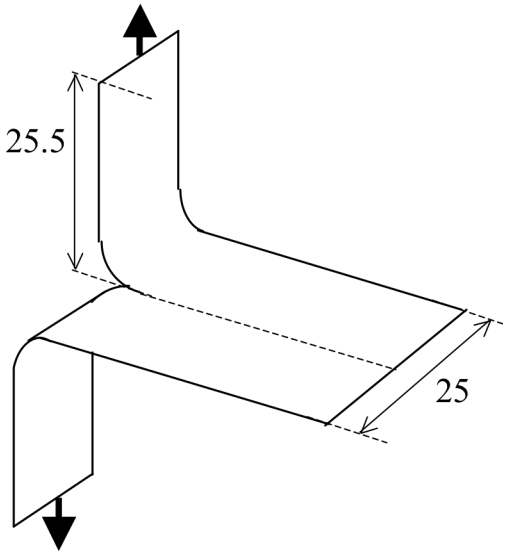


**(a)**

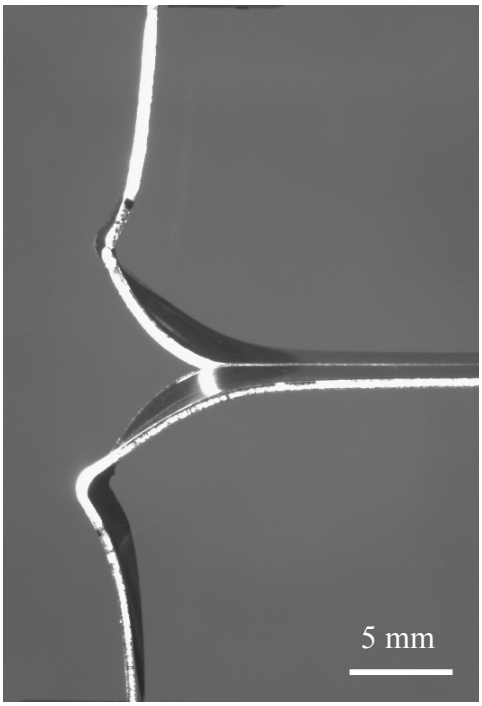


**(b)**

Figure 8

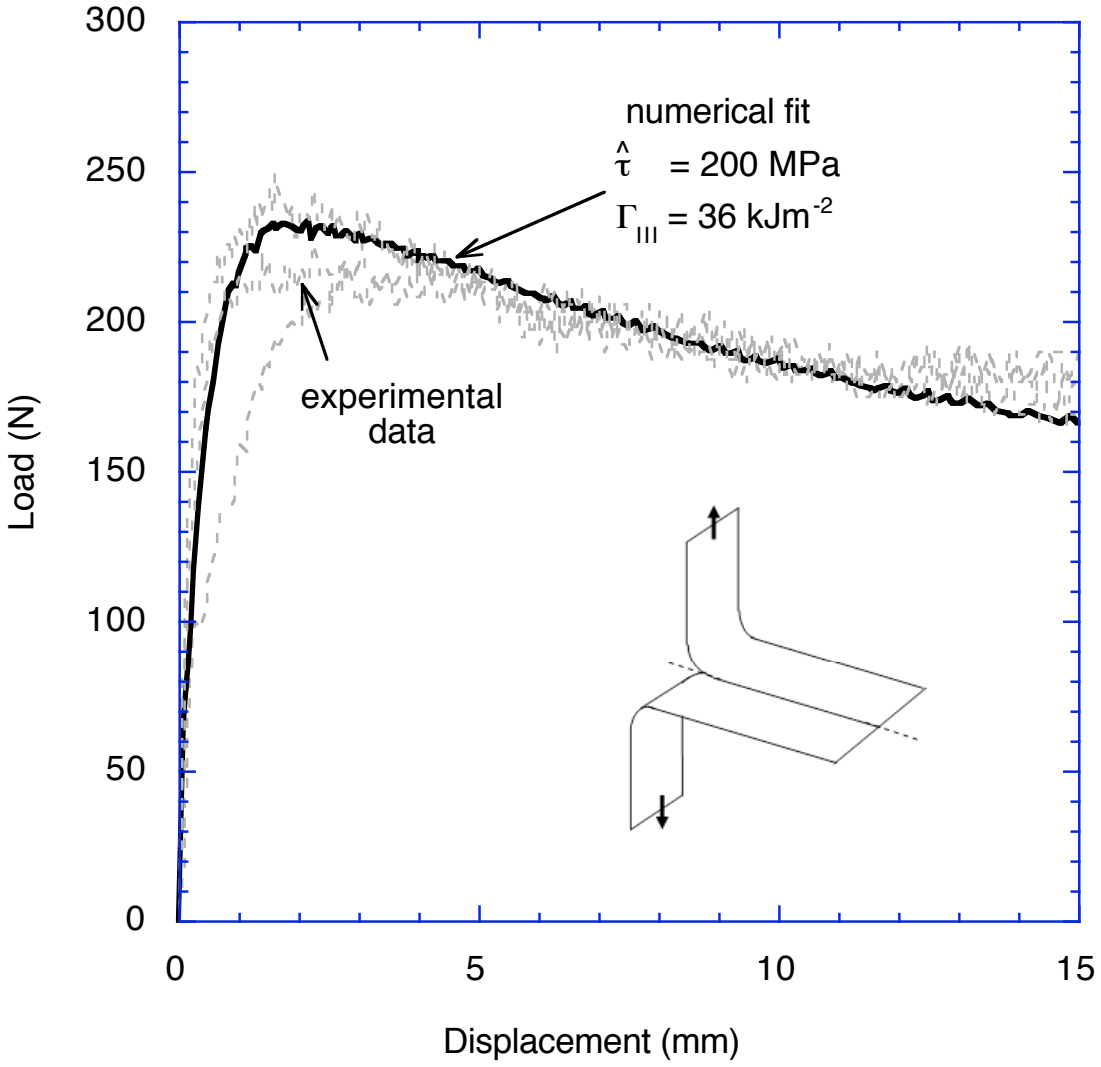
300
250
200
150
100
50
0
Load (N)
0
5
10
15
Displacement (mm)
numerical fit
$\hat{\tau}$ = 200 MPa
$\Gamma_{III}$ = 36 kJm$^{-2}$
experimental
data

Figure 9a

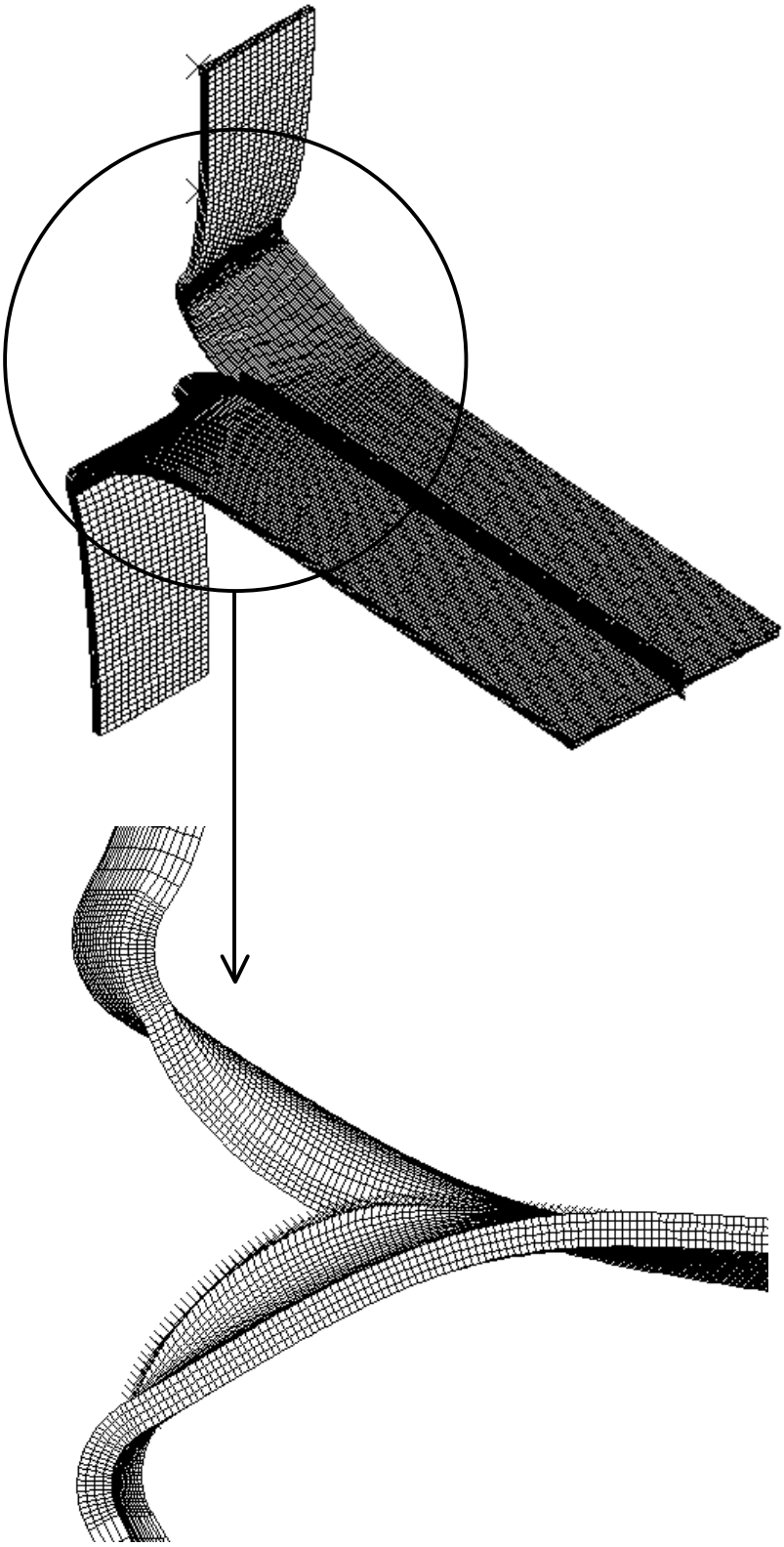

Figure 9b

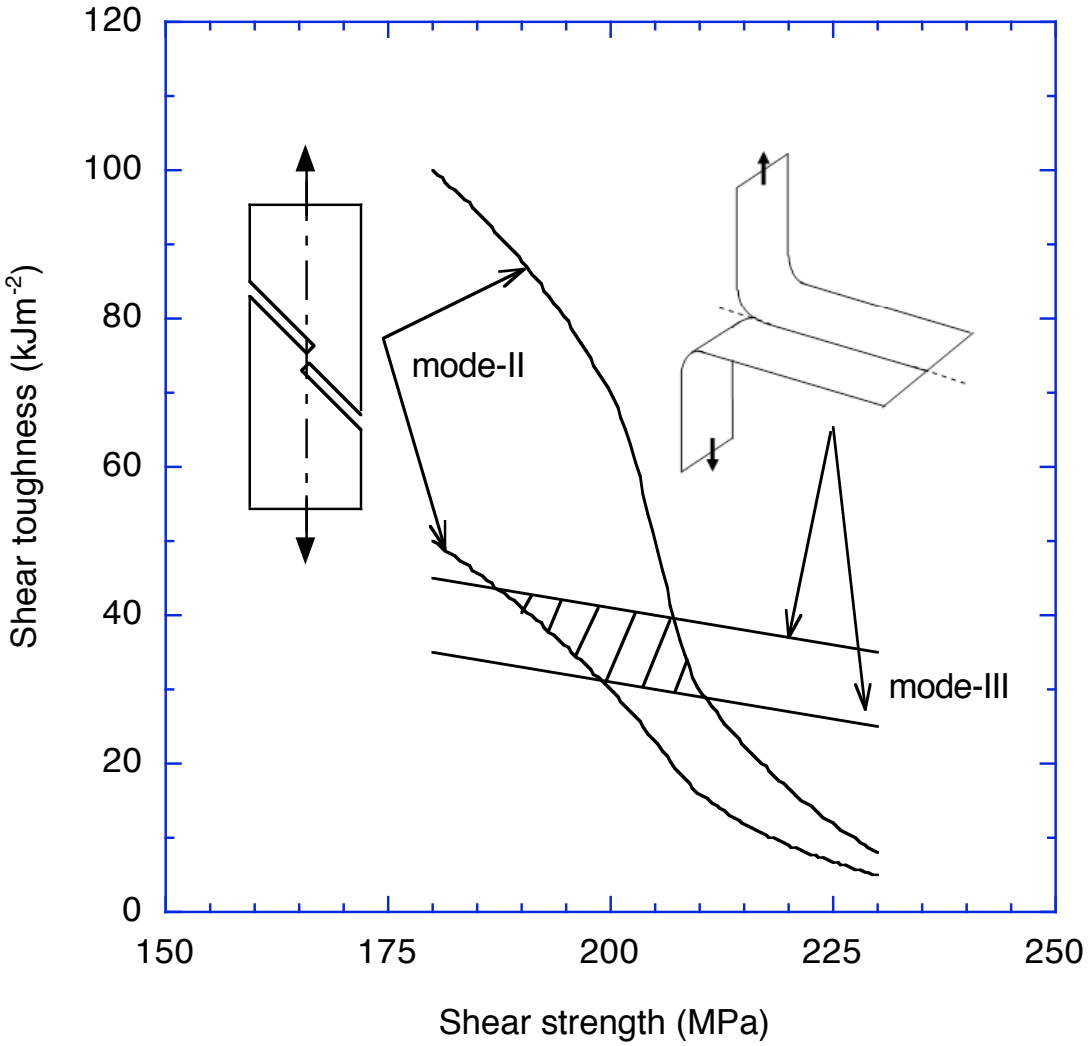
120
100
80
60
40
20
0
150
175
200
225
250
Shear toughness (kJm-2)
Shear strength (MPa)
mode-II
mode-III

Figure 10

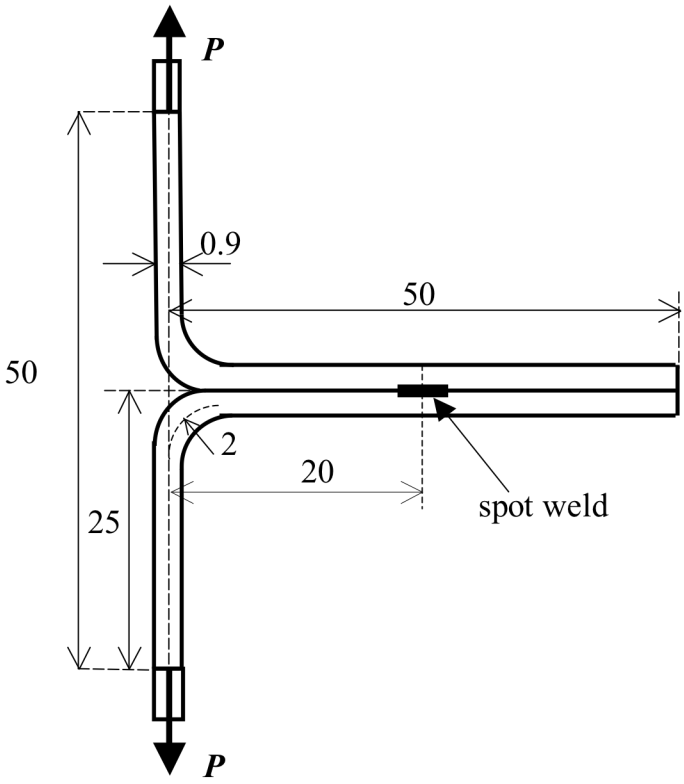


Figure 11

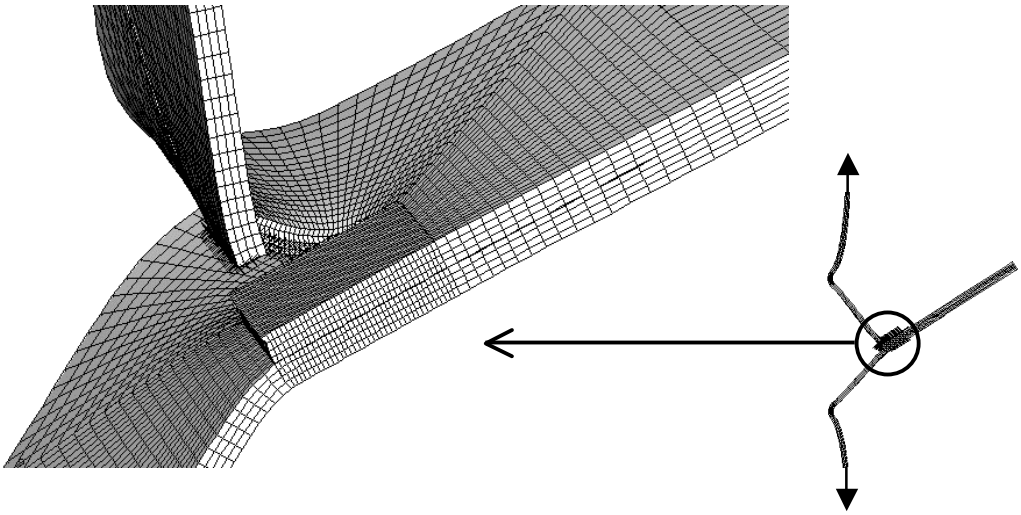

Figure 12a

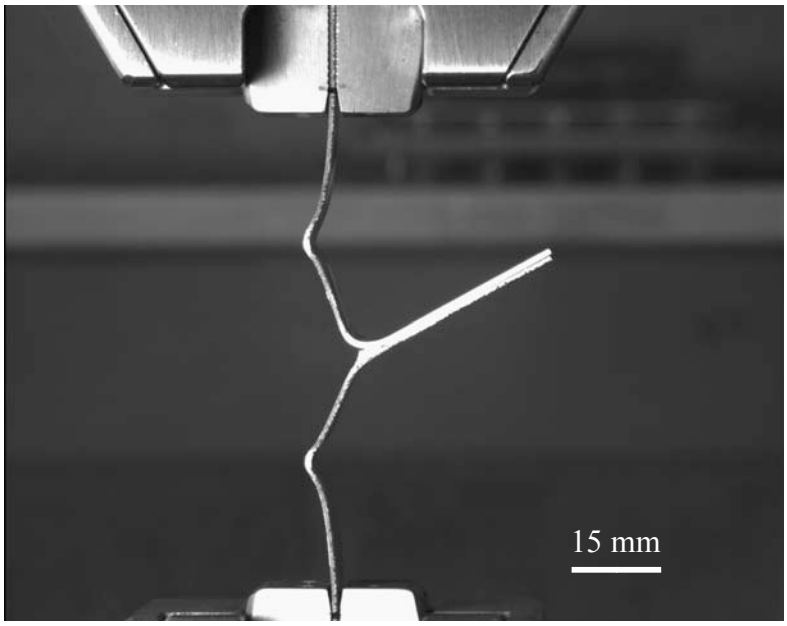


**(b)**

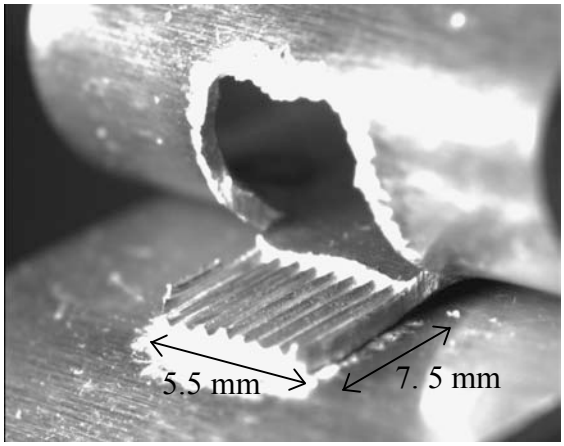


**(c)**

Figure 12

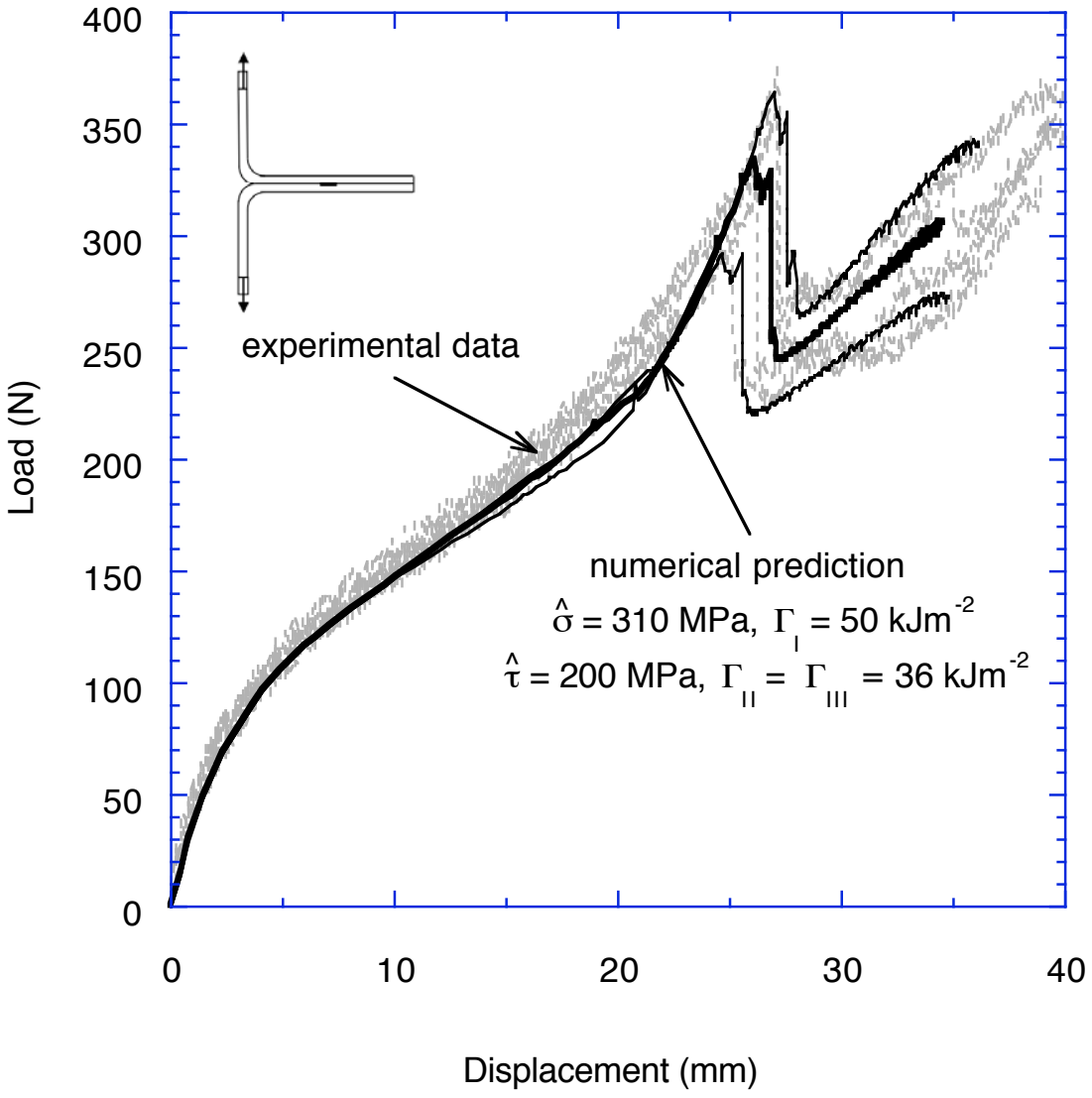
400
350
300
250
200
150
100
50
0
Load (N)
0
10
20
30
40
Displacement (mm)
experimental data
numerical prediction
$\hat{\sigma}$ = 310 MPa, $\Gamma_I$ = 50 kJm$^{-2}$
$\hat{\tau}$ = 200 MPa, $\Gamma_{II}$ = $\Gamma_{III}$ = 36 kJm$^{-2}$

Figure 13

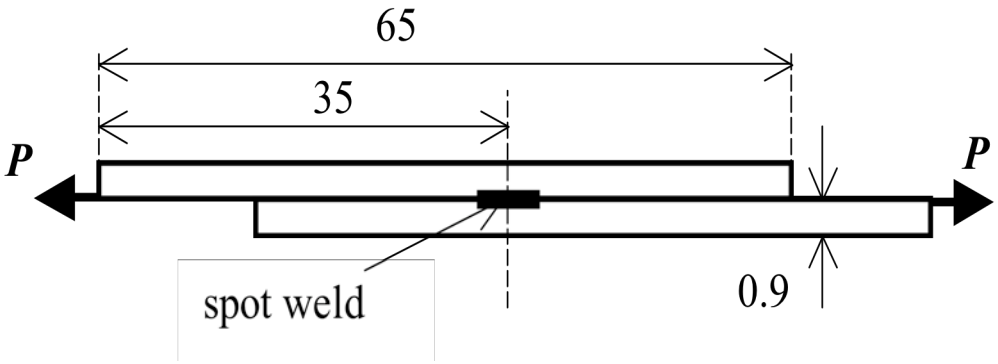


**(a)**

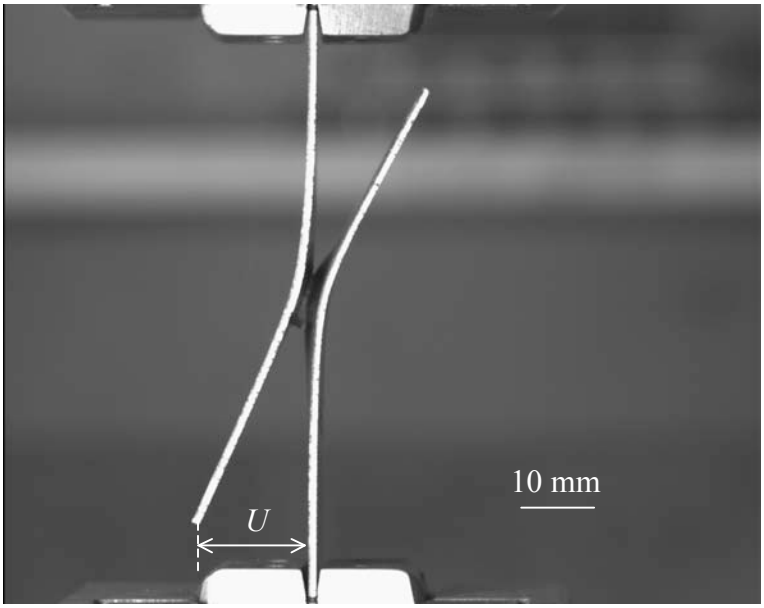


**(b)**

Figure 14

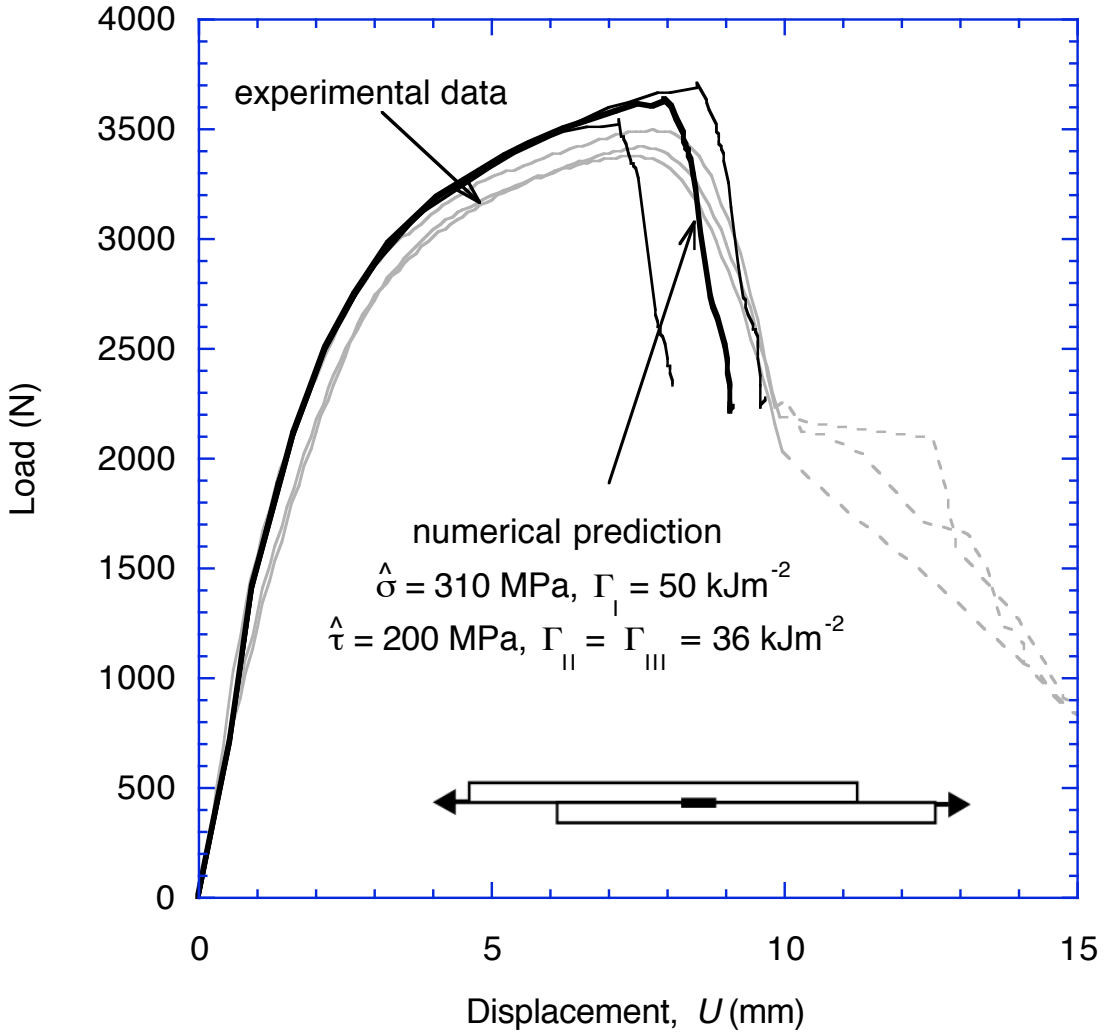
experimental data
numerical prediction
$\hat{\sigma}$ = 310 MPa, $\Gamma_I$ = 50 kJm$^{-2}$
$\hat{\tau}$ = 200 MPa, $\Gamma_{II}$ = $\Gamma_{III}$ = 36 kJm$^{-2}$
Load (N)
Displacement, U (mm)
0
500
1000
1500
2000
2500
3000
3500
4000
0
5
10
15

Figure 15

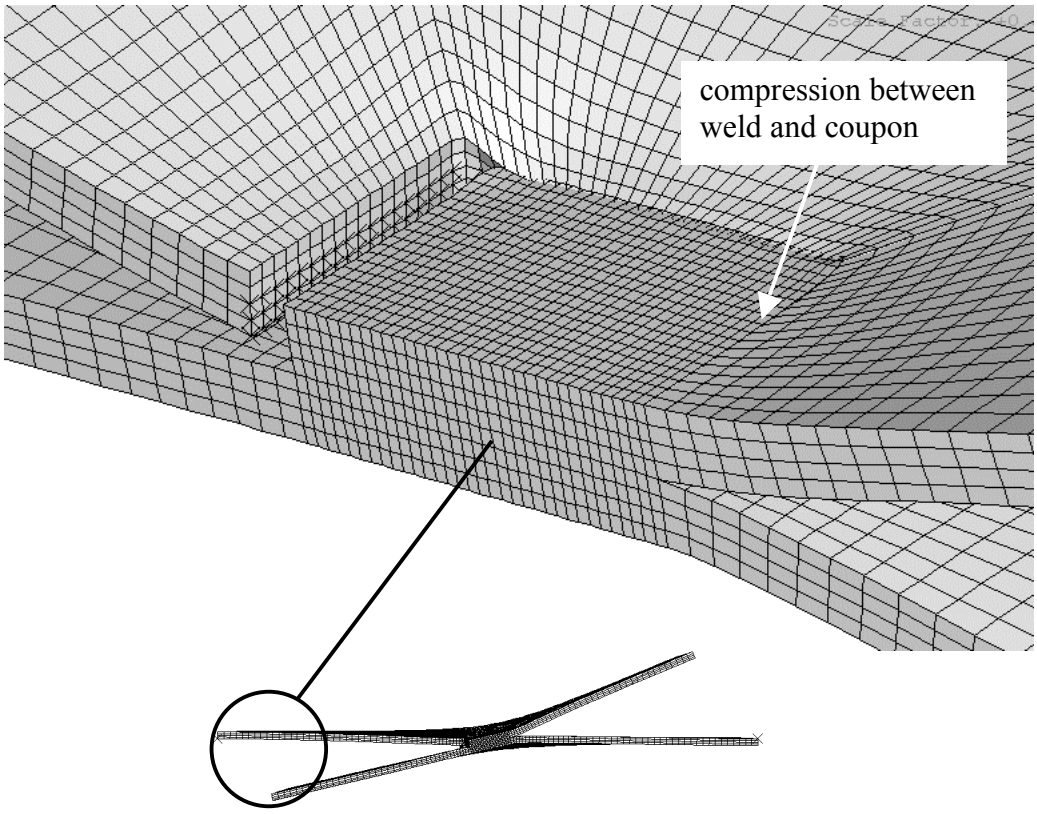
compression between
weld and coupon

**(a)**

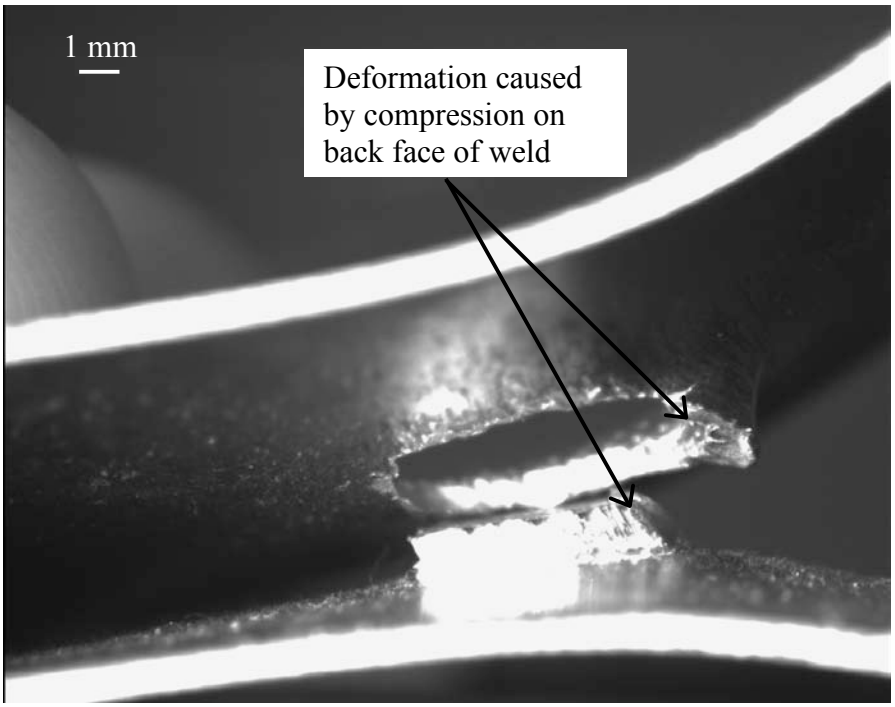
1 mm
Deformation caused
by compression on
back face of weld

**(b)**

Figure 16